Tetrafluorophosphite, PF₄⁻, Anion[†]

Karl O. Christe,[*,1] **David A. Dixon,**[2] **Hélène P. A. Mercier,**[3] **Jeremy C. P. Sanders,**[3] **Gary J. Schrobilgen,**[*,3] **and William W. Wilson**[1]

Contribution from Rocketdyne, A Division of Rockwell International,
Canoga Park, California 91309, Department of Chemistry, McMaster University,
Hamilton, Ontario L8S 4MI, Canada, and Central Research and Development
Department, E. I. du Pont de Nemours and Company, Inc., Experimental Station,
Wilmington, Delaware 19880-0328

Received July 19, 1993[●]

Abstract: $N(CH_3)_4^+PF_4^-$, the first example of a PF_4^- salt, has been prepared from $N(CH_3)_4F$ and PF_3 using either CH_3CN, CHF_3, or excess PF_3 as a solvent. The salt is a white, crystalline solid which is thermally stable up to 150 °C, where it decomposes to $N(CH_3)_3$, CH_3F, and PF_3. The structure of the PF_4^- anion was studied by variable temperature ^{31}P and ^{19}F NMR spectroscopy, infrared and Raman spectroscopy, SCF, MP2, local and nonlocal density functional calculations, a normal coordinate analysis, and single-crystal X-ray diffraction. The anion possesses a pseudo trigonal bipyramidal structure with two longer axial bonds and an equatorial plane containing two shorter equatorial bonds and a sterically active free valence electron pair. In solution, it undergoes an intramolecular exchange process by the way of a Berry pseudorotation mechanism. The vibrational frequencies observed for PF_4^- in solid $N(CH_3)_4PF_4$ are in excellent agreement with those calculated for free gaseous PF_4^-. The X-ray diffraction study (tetragonal, space group $P\bar{4}2_1m$, $a = 8.465(3)$ Å, $c = 5.674(2)$ Å, $Z = 2$, $R = 0.0723$ for 268 observed $[F \geq \sigma(F)]$ reflections suffers from a 3-fold disorder with unequal occupancy factors for the equatorial fluorine atoms of PF_4^- but confirms its pseudo trigonal bipyramidal structure and the axial P–F bond length calculated for the free ion.

Introduction

Although PBr_4^{-4-6} and PCl_4^{-7} salts have been well-known for many years, and the free PF_4^- anion has been observed by mass spectroscopy[8–10] and in ion cyclotron resonance experiments,[11,12] no reports on the isolation of PF_4^- salts could be found in the literature. The only published attempts to prepare such salts were negative. In 1955 Woolf reported that PF_3, when passed over KF *in vacuo* at temperatures up to 240 °C, did not form a salt and that KF and PF_3 at atmospheric pressure and temperatures above 200 °C produced KPF_6 and red phosphorus in an apparent disproportionation reaction.[13] Similarly, Muetterties and co-workers stated[14] in 1960 that KF or CsF absorbs PF_3 at about 150 °C, but that the products were a mixture of PF_6^- salts and red phosphorus and not PF_4^- salts. In 1981, Wermer and Ault reported[15] the isolation of the $Cs^+PF_4^-$ ion pair by codeposition of CsF and PF_3 in an argon matrix; however, their evidence for the presence of such an ion pair is weak since only infrared spectra between about 800 and 550 cm^{-1} were presented, too many bands were observed, and their frequencies do not

correspond well to those found in this study for the PF_4^- anion in $N(CH_3)_4PF_4$.

This lack of evidence for PF_4^- salts in the previous literature was surprising since the F$^-$ affinity of PF_3 (40.2 kcal mol^{-1})[12] is comparable to that of SO_2 (43.8 kcal mol^{-1}),[12] which readily forms stable SO_2F^- salts. Since our recent synthesis[16] of truly anhydrous $N(CH_3)_4F$ had provided us with a source of soluble fluoride ion in combination with a large and relatively inert stabilizing counter cation, we decided to explore whether salts containing the PF_4^- anion could be prepared.

Experimental Section

Apparatus and Materials. Volatile materials were handled in a flamed-out Pyrex glass vacuum line that was equipped with Kontes glass–Teflon valves and a Heise pressure gauge. Nonvolatile materials were handled in the dry nitrogen atmosphere of a glovebox. The infrared and Raman spectrometers and the X-ray diffractometer have previously been described.[17]

Literature methods were used for the syntheses of $N(CH_3)_4F$[16] and the drying of CH_3CN.[18] PF_3 (Ozark Mahoning) and CHF_3 (The Matheson Co.) were purified by fractional condensation prior to their use.

Synthesis of $N(CH_3)_4PF_4$. Three modifications were used for the preparation of this compound, and all three methods gave quantitative yields of the desired $N(CH_3)_4PF_4$ salt.

I. $N(CH_3)_4F$ was loaded in the drybox into a two-piece Pyrex ampule that was closed by a Teflon valve. The vessel was connected to the vacuum line and cooled to −196 °C, and about 4 mL of liquid CH_3CN was added per millimole of $N(CH_3)_4F$. The mixture was briefly warmed to room temperature to dissolve the $N(CH_3)_4F$ and cooled again to −196 °C for the addition of a 50% excess of PF_3. The mixture was allowed to warm to ambient temperature for several hours, and then the volatile products were pumped off, leaving behind white, solid $N(CH_3)_4PF_4$.

† Dedicated to Professor Wolfgang Sawodny on the occasion of his 60th birthday.

● Abstract published in *Advance ACS Abstracts,* February 1, 1994.

(1) E. I. du Pont de Nemours and Company, Inc.

(2) McMaster University.

(3) Rockwell International, Rocketdyne Division.

(4) Dillon, K. B.; Waddington, T. C. *J. Chem. Soc., Chem. Commun.* **1969**, 1317.

(5) Sheldrick, W. S.; Schmidpeter, A.; Zwaschka, F.; Dillon, K. B.; Platt, A. W. G.; Waddington, T. C. *J. Chem. Soc., Dalton Trans.* **1981**, 413.

(6) Sheldrick, W. S.; Kiefer, J. *Z. Naturforsch., B* **1989**, *44B*, 609.

(7) Dillon, K. B.; Platt, A. W. G.; Schmidpeter, A.; Zwaschka, F.; Sheldrick, W. S. *Z. Anorg. Allg. Chem.* **1982**, *488*, 7.

(8) Dillard, J. G.; Rhyne, T. C. *J. Am. Chem. Soc.* **1969**, *91*, 6521.

(9) Rhyne, T. C.; Dillard, J. G. *Inorg. Chem.* **1971**, *10*, 730.

(10) Lane, K. R.; Sallans, L.; Squires, R. R. *J. Am. Chem. Soc.* **1985**, *107*, 5369.

(11) Sullivan, S. A.; Beauchamp, J. L. *Inorg. Chem.* **1978**, *17*, 1589.

(12) Larson, J. W.; McMahon, T. B. *J. Am. Chem. Soc.* **1983**, *105*, 2944.

(13) Woolf, A. A. *J. Chem. Soc.* **1955**, 279.

(14) Muetterties, E. L.; Bither, T. A.; Farlow, M. W.; Coffman, D. D. *J. Inorg. Nucl. Chem.* **1960**, *16*, 52.

(15) Wermer, P.; Ault, B. S. *Inorg. Chem.* **1981**, *20*, 970.

(16) Christe, K. O.; Wilson, W. W.; Wilson, R. D.; Bau, R.; Feng, J. *J. Am. Chem. Soc.* **1990**, *112*, 7619.

(17) Christe, K. O.; Curtis, E. C.; Dixon, D. A.; Mercier, H. P.; Sanders, J. C. P.; Schrobilgen, G. J. *J. Am. Chem. Soc.* **1991**, *113*, 3351.

(18) Christe, K. O.; Dixon, D. A.; Mahjoub, A. R.; Mercier, H. P. A.; Sanders, J. C. P.; Seppelt, K.; Schrobilgen, G. J.; Wilson, W. W. *J. Am. Chem. Soc.* **1993**, *115*, 2696.

Tetrafluorophosphite, PF₄⁻, Anion

J. Am. Chem. Soc., Vol. 116, No. 7, 1994 2851

II. The $N(CH_3)_4F$ was dissolved in liquid CHF_3 at -78 °C, using about 2 g of CHF_3 per millimole of $N(CH_3)_4F$, followed by the addition of twice the required amount of PF_3 at -196 °C. The mixture was warmed for about 10 h to -78 °C, followed by the pumping off of all material that was volatile at room temperature. The white solid residue consisted of $N(CH_3)_4PF_4$.

III. The $N(CH_3)_4F$ was placed into a small volume, stainless steel Hoke cylinder that was closed by a valve. On the vacuum line, a 15-fold excess of PF_3 was added to the cylinder at -196 °C, and the cylinder was kept at room temperature for 12 h. The cylinder was cooled again to -196 °C, and all volatile material was removed by pumping during warm-up of the cylinder from -196 °C to room temperature, leaving behind the white solid $N(CH_3)_4PF_4$.

Pyrolysis of $N(CH_3)_4PF_4$. A sample of $N(CH_3)_4PF_4$ (1.68 mmol) in a Pyrex vessel was heated in a dynamic vacuum at 165 °C for 6.5 h. The volatile decomposition products consisted of PF_3 (1.51 mmol), CH_3F (0.92 mmol), and $N(CH_3)_3$ (0.92 mmol), in good agreement with the observed weight loss. The beige-colored residue (85 mg) was identified by infrared and ^{19}F NMR spectroscopy as a mixture of $N(CH_3)_4^+$ salts of PF_6^-, HPF_5^-, and POF_2^-. Differential scanning calorimetry (DSC) showed three irreversible endotherms for $N(CH_3)_4PF_4$, a very small one at 158 °C, a medium one at about 238 °C, and a large one at about 246 °C.

Crystal Structure Determination of $N(CH_3)_4PF_4$. Single crystals of $N(CH_3)_4PF_4$ were obtained from a CH_3CN solution, saturated at 50 °C, by allowing the solution in a Teflon–FEP vessel to cool slowly to room temperature. Large transparent crystals were obtained that were square plates and grew as clusters. The crystal used had the dimensions of 0.3 × 0.3 × 0.05 mm.

The crystal was centered on a Siemens R3m/V diffractometer and diffracted only at low angles because of its dimensions. Accurate cell dimensions were determined at -100 °C from a least-squares refinement of the setting angles (χ, ϕ, and 2θ) obtained from 14 accurately centered reflections (with $5.35° \leq 2\theta \leq 12.77°$). Integrated diffraction intensities were collected using a θ–2θ scan technique with scan rates varying from 1.5 to 14.65°/min (in 2θ) and a scan range of $\pm 0.6°$ so that the weaker reflections were examined more slowly. The data were collected within $0 \leq h \leq 10$, $0 \leq k \leq 10$, and $0 \leq l \leq 6$ and $3 \leq 2\theta \leq 40°$ using Ag $K\alpha$ with a graphite monochromator ($\lambda = 0.56086$ Å). The intensities of three standard reflections were monitored every 97 reflections; no decay was observed. A total of 472 reflections were collected, and 270 unique reflections remained after averaging of equivalent reflections. Lorentz and polarization corrections were applied. The $P\bar{4}2_1m$ space group was obtained from the Laue symmetry, the $0k0$ extinctions with $k \neq 2n$, and the non-centrosymmetric E_s statistics.

The solution was obtained by direct methods.[19] The structure consisted of well separated, ordered $N(CH_3)_4^+$ cations and disordered PF_4^- anions. While the positioning of the $N(CH_3)_4^+$ cation was straightforward (N on $\bar{4}$ and C on 1), the orientation of the PF_4^- anion was problematic since the tetragonal axis of the crystal was incompatible with the expected geometry of the PF_4^- anion. All the atoms of PF_4^- were found on special positions, i.e., P and F(2) on $2.mm$ and F(1) and F(3) on $.mm$, requiring disorder of the equatorial fluorines. The assumption of 2-fold disorder (structures a + b given in the Results and Discussion section) along the equatorial P–F(2) axis, i.e., of a positional disorder of one equatorial fluorine atom and the sterically active free valence electron pair on phosphorus, and of site occupancy factors (sof) of 0.25 for both F(2) and F(3), gave R-factors of 0.0876 with 268 reflections and of 0.0544 with 185 reflections.

A second disorder model assuming 3-fold disorder along the axial F(1)–P–F(1) axis with equal occupancy factors of 0.1667 for the three equatorial F positions (structures a + b + c given in the Results and Discussion section) gave R-factors of 0.0867 with 268 reflections and 0.0539 with 185 reflections but did not result in the required equal bond lengths for the three equatorial P–F bonds and the 120° and 180° bond angles for the equatorial and axial PF_2 groups, respectively. Instead, the geometry found was similar to that found under the assumption of 2-fold disorder.

A third model was tested with variable proportions of structures (a + b) and c, while maintaining the sum of the sof's of F(2) and F(3) equal to 0.5. Minimum R-values of 0.0723 with 268 reflections and 0.0510 with 185 reflections were obtained with sof's of 0.20 for F(2) and 0.30 for F(3).

(19) Sheldrick, G. M. *SHELXTL PLUS*, Release 4.21/V; Siemens Analytical X-Ray Instruments, Inc.: Madison, WI, 1990.

Table 1. Summary of Crystal Data and Refinement Results for $N(CH_3)_4PF_4$

space group	$P\bar{4}2_1m$
a	8.465(3) Å
c	5.674(2) Å
V (Å³)	406.5(2)
molecules/unit cell	2
mol wt (g mol⁻¹)	181.1
calcd density (g cm⁻³)	1.480
T (°C)	-100
μ (cm⁻¹)	1.8
wavelength (Å) used for data collcn	0.560 86
final agreement factors	$R = 0.0723$
	$R_w = 0.0745$

Table 2. Atomic Coordinates (× 10⁴) and Equivalent Isotropic Displacement Coefficients (Å² × 10³) in $N(CH_3)_4^+PF_4^-$

	x	y	z	$U(eq)^a$	sof^b
P	5000	0	3962(6)	60(1)	0.25
F(1)	3567(4)	1433(4)	4016(11)	65(2)	0.50
F(2)	5000	0	6645(13)	53(2)	0.20
F(3)	−1087(11)	6087(11)	6759(29)	101(4)	0.30
N	0	0	0	33(2)	0.25
C	1450(6)	104(8)	−1526(8)	42(1)	1.00

^{a} Equivalent isotropic U defined as one-third of the trace of the orthogonalized U_{ij} tensor. ^{b} Site occupancy factor.

Table 3. A Comparison of the Apparent Interactive Distances (Å) and Bond Angles (deg) of PF_4^- from the X-ray Diffraction Study with Those Calculated at the SCF Level for Free Ordered PF_4^- and with the Apparent Geometries of the Free Ion When Subjected to Either 2-Fold or 3-Fold Disorder with Equal Occupancy Factors

	apparent geometry from crystal structure	calcd geometries of the free ion		
		ordered	2-fold disordered	3-fold disordered
P–F(1)$_{ax}$	1.716(1) [1.726]^a	1.741	1.736	1.741
P–F(2)$_{eq}$	1.522(8) [1.559]	1.604	1.604	<1.604
P–F(3)$_{eq}$	1.386(5) [1.410]	1.604	<1.604	
F(2)–P–F(3)	108.0(5)	99.9	99.9	120
F(1)–P–F(1)	178.0(5)	168.3	172.4	180
F(1)–P–F(2)	89.0(2)	86.2	86.2	90
F(1)–P–F(3)	90.3(6)	86.2	90.4	90
F(3)–P–F(3A)	143.9(12)		160.2	120

^{a} The values in square brackets have been corrected for libration.

The possibility of disorder higher than 3, such as the 8-fold disorder found for BF_4^- in $N(CH_3)_4BF_4$,[20] was also examined but was found to be incompatible with the symmetry requirements of our preferred space group. Furthermore, the Fourier difference map revealed no significant electron density in the equatorial plane after subtraction of the phosphorus and the three original equatorial fluorine positions. In the final difference Fourier map, the maximum and minimum electron densities were 0.92 and -0.58 e Å⁻³, with the maximum located near the P atom.

A summary of the crystal data and refinement results for the 3-fold disordered model with unequal occupancy factors, the final atomic coordinates, equivalent isotropic thermal parameters and site occupancy factors, and the important apparent bond lengths and angles for the PF_4^- anion are given in Tables 1–3. The apparent bond lengths corrected for librational motion are also given in Table 3 and are used throughout the following discussion. A summary of the structure determination, anisotropic displacement coefficients, H-atom coordinates and their isotropic displacement coefficients, and the observed and calculated structure factors are given in the supplementary material, Tables S1–S4.

Nuclear Magnetic Resonance Spectroscopy. The ^{19}F and ^{31}P NMR spectra were recorded unlocked (field drift < 0.1 Hz h⁻¹) on a Bruker AM-500 spectrometer equipped with an 11.744T cryomagnet. Temperatures were measured with a copper–constantan thermocouple inserted directly into the sample region of the probe and were considered accurate to ± 1 °C. The spectra were referenced to neat external samples of $CFCl_3$(^{19}F) and 85% H_3PO_4(^{31}P) at ambient temperature. The IUPAC chemical shift convention was used.

Samples for ^{31}P NMR spectroscopy were prepared in 9-mm-o.d. FEP NMR tubes as described previously[17] using a 2.4-fold excess of $N(CH_3)_4F$

(20) Giuseppetti, G.; Mazzi, F.; Tadini, C. *Z. Kristallogr.* **1992**, *202*, 81.

and CH₃CN as a solvent. The ¹⁹F NMR samples were prepared in an analogous fashion using 4-mm-o.d. FEP NMR tubes and a 3.7-fold excess of N(CH₃)₄F and CH₃CN (0.25 mL).

Computational Methods. The density functional theory[21] calculations were done with the programs DGauss,[22] which employs Gaussian orbitals, and DMol,[23] which employs numerical orbitals, on a Cray YMP computer. In DGauss, the local potential of Vosko, Wilk, and Nusair[24] is used. The calculations were done at the self-consistent nonlocal level with the nonlocal exchange potential of Becke[25] together with the nonlocal correlation functional of Perdew.[26] The basis set on P has the form (7321/621/1) and that on F has the form (721/621/1).[27] The fitting basis has the form (9/4/4) for P and (7/3/3) for F.

The DMol calculations were done with a polarized double-ζ numerical basis set,[18] using the local potential of von Barth and Hedin.[28] Geometries were optimized by using analytical gradients.[22] Second derivatives were calculated by numerical differentiation of the analytic first derivatives. A two-point method with a finite difference of 0.01 au was used.

The ab initio molecular orbital calculations were done with the program systems GRADSCF[29] and Gaussian 92[30] on a Cray YMP computer. The geometries were optimized by using analytic gradient methods[31] at the SCF and MP2 levels.[32] Force fields were also evaluated analytically[33] at the SCF and MP2 levels. The basis sets are of polarized double-ζ quality for P[34] and F.[35]

Results and Discussion

Synthesis and Properties of N(CH₃)₄PF₄. The synthesis of N(CH₃)₄PF₄, the first known example of a PF₄⁻ salt, was achieved

according to eq 1. The salt is formed in quantitative yield by

$$N(CH_3)_4F + PF_3 \rightarrow N(CH_3)_4PF_4 \qquad (1)$$

reacting an excess of PF₃ with N(CH₃)₄F in a suitable solvent such as CH₃CN at room temperature, CHF₃ at −78 °C, or liquid PF₃ either at or below room temperature. Due to the relatively low boiling points of CHF₃ and PF₃, the synthesis in CH₃CN solution is preferred and can be carried out in standard glassware. Attempts to prepare CsPF₄ from CsF and liquid PF₃ at room temperature were unsuccessful. The only observed reaction product was a small amount of CsPF₆.

The N(CH₃)₄PF₄ salt is a white crystalline salt which is stable up to about 150 °C, at which temperature it starts to slowly decompose according to eqs 2 and 3, with eq 2 being faster than eq 3.

$$N(CH_3)_4PF_4 \rightarrow N(CH_3)_4F + PF_3 \qquad (2)$$

$$N(CH_3)_4F \rightarrow N(CH_3)_3 + CH_3F \qquad (3)$$
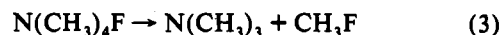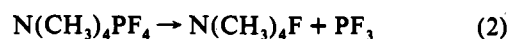
The successful synthesis of the PF₄⁻ anion and its good thermal stability are in accord with the high F⁻ affinity of PF₃ (40.2 kcal mol⁻¹)[12] and was made possible by the availability of a soluble, anhydrous F⁻ ion source, i.e., N(CH₃)₄F.[16] The use of anhydrous and hydroxyl- and HF-free conditions is important in view of PF₄⁻ undergoing the following facile reactions 4–8. These reac-

$$2PF_4^- + 2H_2O \rightarrow HPF_5^- + HPO_2F^- + 2HF \qquad (4)$$

$$PF_4^- + H_2O + 2N(CH_3)_4F \rightarrow POF_2^- + 2N(CH_3)_4HF_2 \qquad (5)$$

$$PF_4^- + CH_3OH \rightarrow PF_2(OCH_3) + HF_2^- \qquad (6)$$

$$PF_4^- + 2CH_3OH \rightarrow PF(OCH_3)_2 + HF + HF_2^- \qquad (7)$$

$$PF_4^- + HF \rightarrow HPF_5^- \qquad (8)$$
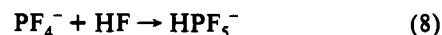
tions have been studied in detail by multinuclear NMR and vibrational spectroscopy and will be discussed in a separate publication.[36]

³¹P and ¹⁹F NMR Spectroscopy of the PF₄⁻ Anion. The ³¹P NMR spectrum of N(CH₃)₄PF₄ in CH₃CN at −40 °C reveals a broad singlet ($\Delta\nu_{1/2}$ = 163 Hz) at δ = 42.3 ppm. The lack of fine structure indicates that the PF₄⁻ anion undergoes relatively fast intermolecular exchange under these conditions. However, when a 1.5 M excess of N(CH₃)₄F is added to the sample, the intermolecular exchange is slowed down and the ³¹P NMR spectrum at −46 °C (Figure 1) reveals a triplet of triplets at δ = 40.5 ppm. This is in agreement with the pseudo trigonal bipyramidal structure expected for PF₄⁻ according to the VSEPR model.[37,38] The coupling pattern arises from the coupling of the phosphorus to the two inequivalent sets of fluorine ligands: $^1J(^{31}P-^{19}F_{ax})$ = 660 Hz and $^1J(^{31}P-^{19}F_{eq})$ = 1405 Hz. Six of the inner lines of the multiplet are broader than the central and two outer lines. This pattern is indicative of the PF₄⁻ anion undergoing an intramolecular ligand exchange process in which both equatorial and axial ligands interchange at the same time.[39] In order to confirm this, a series of variable temperature ³¹P NMR spectra

(21) (a) Parr, R. G.; Yang, W. *Density Functional Theory of Atoms and Molecules*; Oxford University Press: New York, 1989. (b) Salahub, D. R. In *Ab Initio Methods in Quantum Chemistry-II*; Lawley, K. P., Ed.; J. Wiley & Sons: New York, 1987; p 447. (c) Wimmer, E.; Freeman, A. J.; Fu, C.-L.; Cao, P.-L.; Chou, S.-H.; Delley, B. In *Supercomputer Research in Chemistry and Chemical Engineering*; Jensen, K. F., Truhlar, D. G., Eds.; ACS Symposium Series 353; American Chemical Society: Washington, DC, 1987; p 49. (d) Jones, R. O.; Gunnarsson, O. *Rev. Mod. Phys.* **1989**, *61*, 689. (e) Ziegler, T. *Chem. Rev.* **1991**, *91*, 651.

(22) (a) Andzelm, J.; Wimmer, E.; Salahub, D. R. In *The Challenge of d and f Electrons: Theory and Computation*; Salahub, D. R., Zerner, M. C., Eds.; ACS Symposium Series 394; American Chemical Society: Washington, DC, 1989; p 228. (b) Andzelm, J. In *Density Functional Methods in Chemistry*; Labanowski, J., Andzelm, J., Eds.; Springer-Verlag: New York, 1991; p 101. (c) Andzelm, J.; Wimmer, E. *J. Chem. Phys.* **1992**, *96*, 1280. (d) DGauss is a local density functional program available via the Cray Research Unichem Project, Cray Research, Eagan, MN, 1993.

(23) (a) Delley, B. *J. Chem. Phys.* **1990**, *92*, 508. (b) Dmol is available commercially from BIOSYM Technologies, San Diego, CA. The multipolar fitting functions for the model density used to evaluate the effective potential have angular momentum numbers of 3 for F and P.

(24) Vosko, S. H.; Wilk, L.; Nusair, M. *Can. J. Phys.* **1980**, *58*, 1200.

(25) (a) Becke, A. D. *Phys. Rev.* **1988**, *A38*, 3098. (b) Becke, A. D. In *The Challenge of d and f Electrons: Theory and Computation*; Salahub, D. R., Zerner, M. C., Eds.; ACS Symposium Series 394; American Chemical Society: Washington, DC, 1989; p 166. (c) Becke, A. D. *Int. J. Quantum Chem. Symp.* **1989**, *23*, 599.

(26) Perdew, J. P. *Phys. Rev. B* **1986**, *33*, 8822.

(27) Godbout, N.; Salahub, D. R.; Andzelm, J.; Wimmer, E. *Can. J. Chem.* **1992**, *70*, 560.

(28) Von Barth, U.; Hedin, L. *J. Phys. C* **1972**, *5*, 1629.

(29) GRADSCF is an ab initio program system designed and written by A. Komornicki at Polyatomics Research.

(30) *GAUSSIAN 92*; Frisch, M. J., Trucks, G. W., Head-Gordon, M., Gill, P. M. W., Wong, M. W., Foresman, J. B., Johnson, B. G., Schlegel, H. B., Robb, M. A., Replogle, E. S., Gomperts, R., Andres, J. L., Raghavachari, K., Binkley, J. S., Gonzalez, C., Martin, R. L., Fox, J., DeFrees, D. J., Baker, J., Stewart, J. J. P., Pople, J. A., Eds.; Gaussian Inc.: Pittsburg, PA, 1992.

(31) (a) Komornicki, A.; Ishida, K.; Morokuma, K.; Ditchfield, R.; Conrad, M. *Chem. Phys. Lett.* **1977**, *45*, 595. (b) McIver, J. W., Jr.; Komornicki, A. *Chem. Phys. Lett.* **1971**, *10*, 303. (c) Pulay, P. In *Applications of Electronic Structure Theory*; Schaefer, H. F., III, Ed.; Plenum Press: New York, 1977; p 153.

(32) (a) Moller, C.; Plesset, M. S. *Phys. Rev.* **1934**, *46*, 618. (b) Pople, J. A.; Binkley, J. S.; Seeger, R. *Int. J. Quantum Chem. Symp.* **1976**, *10*, 1. (c) Pople, J. A.; Krishnan, R.; Schlegel, H. B.; Binkley, J. S. *Int. J. Quantum Chem. Symp.* **1979**, *13*, 325. (d) Handy, N. C.; Schaefer, H. F., III. *J. Chem. Phys.* **1984**, *81*, 5031.

(33) (a) King, H. F.; Komornicki, A. *J. Chem. Phys.* **1986**, *84*, 5645. (b) King, H. F.; Komornicki, A. In *Geometrical Derivatives of Energy Surfaces and Molecular Properties*; Jorgenson, P., Simons, J., Eds.; NATO ASI Series C; D. Reidel: Dordrect, 1986; Vol. 166, p 207.

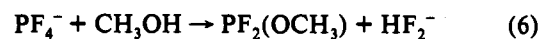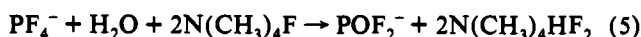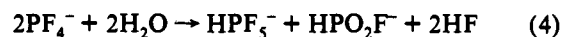(34) McLean, A. D.; Chandler, G. S. *J. Chem. Phys.* **1980**, *72*, 5639. D exponent = 0.50.

(35) Dunning, T. H., Jr.; Hay, P. J. In *Methods of Electronic Structure Theory*; Schaefer, H. F., III, Ed.; Plenum Press: New York, 1977; Chapter 1.

(36) Christe, K. O.; Dixon, D. A.; Sanders, J. C. P.; Schrobilgen, G. J.; Wilson, W. W. To be published.

(37) Gillespie, R. J. *Molecular Geometry*; Van Nostrand Reinhold Co.: London, 1972.

(38) Gillespie, R. J.; Hargittai, I. *The VSEPR Model of Molecular Geometry*; Allyn and Bacon: Boston, 1991.

(39) Steigel, A. In *NMR–Basic Principles and Progress*; Diel, P., Fluck, E., Kosfeld, R., Eds.; 1978; Vol. 15, p 1 and references therein.
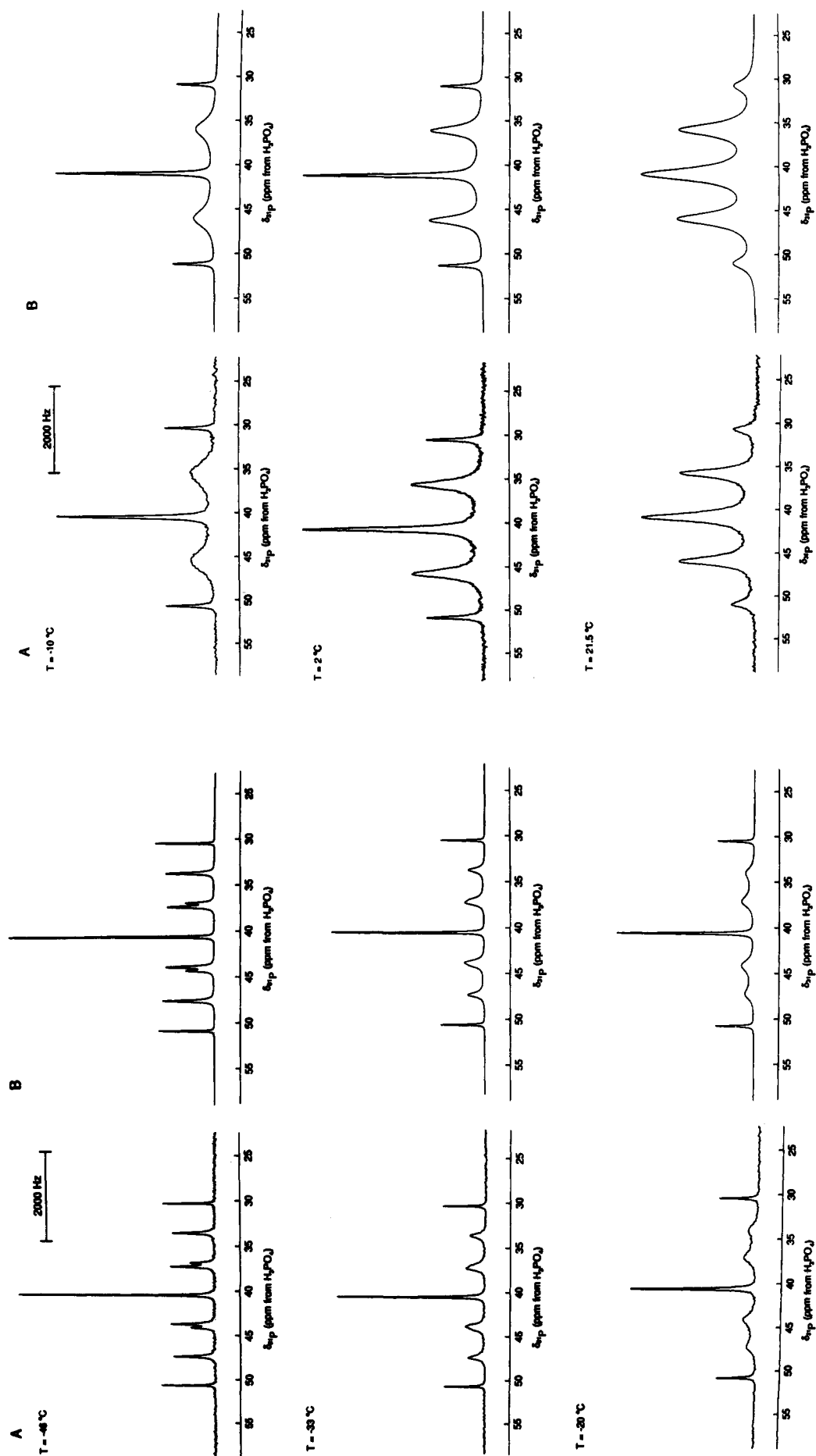
Tetrafluorophosphite, PF₄⁻, Anion

J. Am. Chem. Soc., Vol. 116, No. 7, 1994 2853

Figure 1. Variable temperature ^{31}P NMR spectra (202.459 MHz) for N(CH₃)₄PF₄ in CH₃CN containing a 1.5 M excess of N(CH₃)₄F: (A) observed spectra; (B) calculated spectra.

Table 4. Exchange Rate Data Extracted from Variable Temperature ^{31}P NMR Spectra of $N(CH_3)_4PF_4$ Dissolved in CH_3CN Containing a 1.5 M Excess of $N(CH_3)_4F$

T, K	k, s^{-1} × 10^2	T, K	k, s^{-1} × 10^2
227	1.00	250	8.50
233	1.60	260	25.0
240	3.10	275	56.0

were obtained over the range –46 to 21 °C (Figure 1). The observed changes in the multiplet pattern on raising the temperature are analogus to those found in the XPF$_4$ series of molecules (where X = $N(CH_3)_2$, Cl, or CH$_3$)[40] and are consistent with a mechanism in which both equatorial and axial ligands interchange simultaneously.[39,40] The ^{31}P NMR spectra measured at the highest temperatures reveal significant broadening of the multiplet components as a result of intermolecular fluoride exchange, and in addition, the samples turned orange in color due to attack of the excess F$^-$ on the CH$_3$CN solvent.[41] The mechanism by which the intramolecular ligand exchange process occurs in PF$_4^-$ is most likely the classical Berry pseudorotation mechanism[42] involving a pyramidal C_{4v} transition state with four equivalent fluorine positions.[43]

C$_{2v}$ C$_{4v}$ C$_{2v}$
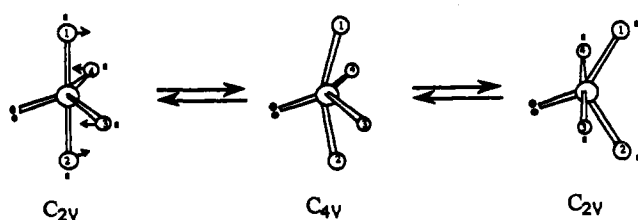
However, it should be noted that NMR spectroscopy alone could not distinguish between this and other mechanisms that result in the same permutation of fluorine nuclei.[39,40] Other mechanisms have been favored for compounds such as ClF$_3$,[44] which possesses two free valence electron pairs on the central atom, or SiH$_4$F$^-$ [45] and PH$_4$F,[46] where in the minimum energy structures, the two axial positions are occupied by one fluorine and one hydrogen ligand. For PF$_4^-$, the rate constants have been determined at different temperatures by visual matching of the experimental spectra with those generated by the DNMR 3 simulation program[47] for exchanging systems (See Table 4). Using previously established equations[48] and an Eyring plot of the rate data (Figure 2), $\Delta H^{\ddagger}$ and $\Delta S^{\ddagger}$ were determined to be 43 ± 2 kJ mol and –13 ± 2 J K^{-1} mol^{-1}, respectively. These values compare well with values obtained for the intramolecular exchange process in the isoelectronic SF$_4$ molecule[49-51] and the theoretical value for $\Delta H^{\ddagger}$ (see Theoretical Calculations section). For SF$_4$, the values obtained for purified neat liquid ($\Delta H^{\ddagger}$ = 49.2 kJ mol^{-1}, $\Delta S^{\ddagger}$ = 4.4 J K^{-1} mol^{-1}) and gaseous ($\Delta H^{\ddagger}$ = 51.9 kJ mol^{-1}, $\Delta S^{\ddagger}$ = 9.3 J K^{-1} mol^{-1}) samples of SF$_4$ are regarded as the most reliable,

(40) Eisenhut, M.; Mitchell, H. L.; Traficante, D. D.; Kaufman, R. J.; Deutch, J. M.; Whitesides, G. M. *J. Am. Chem. Soc.* **1974**, *96*, 5385.

(41) Christe, K. O.; Wilson, W. W. *J. Fluorine Chem.* **1990**, *46*, 339.

(42) (a) Berry, R. S. *J. Chem. Phys.* **1960**, *32*, 933. (b) Wasada, H.; Hirao, K. *J. Am. Chem. Soc.* **1992**, *114*, 16.

(43) Gordon, M. S.; Windus, T. L.; Burggraf, L. W.; Davis, L. P. *J. Am. Chem. Soc.* **1990**, *112*, 7167.

(44) Minyaev, R. M. *Chem. Phys. Lett.* **1992**, *196*, 203.

(45) Windus, T. M.; Gordon, M. S.; Burggraf, L. W.; Davis, L. P. *J. Am. Chem. Soc.* **1991**, *113*, 4356.

(46) Windus, T. M.; Gordon, M. S. *Theor. Chim. Acta* **1992**, *83*, 21.

(47) (a) Kleier, D. A.; Binsch, G. *Quantum Chemistry Exchange*; Indiana University: Bloomington, 1969; No. 165. (b) Binsch, G. In *Dynamic NMR Spectroscopy*; Jackman, L. M., Cotton, F. A., Eds.; Academic Press: New York, 1975; p 45.

(48) Günther, H. *NMR Spectroscopy–An Introduction*; J. Wiley and Sons: New York, 1973; Chapter 8, p 240.

(49) Seel, F.; Gombler, W. *J. Fluorine Chem.* **1974**, *4*, 327. Gibson, J. A.; Ibbott, D. G.; Janzen, A. F. *Can. J. Chem.* **1973**, *51*, 3203.

(50) Gombler, W. Diploma Thesis, Saarbrücken, FRG, 1974. Gombler, W. Personal communication.

(51) Spring, C. A.; True, N. S. *J. Am. Chem. Soc.* **1983**, *105*, 7231.
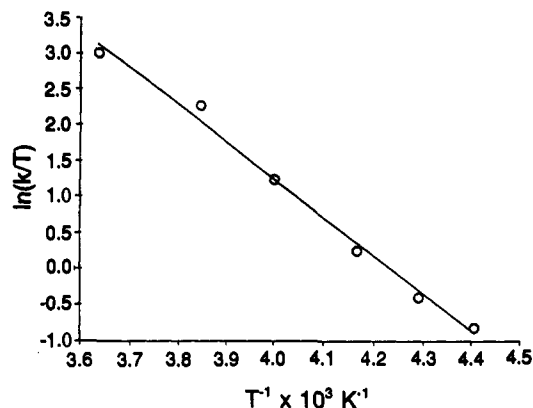
Figure 2. Eyring plot of the exchange rate data extracted from the variable temperature ^{31}P NMR spectra (202.459 MHz) for $N(CH_3)_4PF_4$ in CH$_3$-CN containing a 1.5 M excess of $N(CH_3)_4F$.
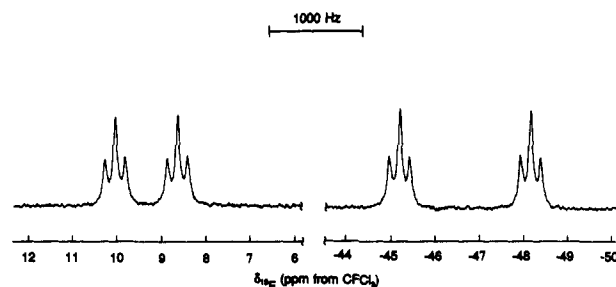
Figure 3. The ^{19}F NMR spectrum (470.599 MHz) at –46 °C of $N(CH_3)_4$-PF$_4$ in CH$_3$CN containing a 1.5 M excess of $N(CH_3)_4F$.

since they represent the highest $\Delta H^{\ddagger}$ and most positive $\Delta S^{\ddagger}$ values.[50,51] The somewhat lower values of $\Delta H^{\ddagger}$ and $\Delta S^{\ddagger}$ obtained for PF$_4^-$ can probably be ascribed to the effects of some intermolecular fluoride exchange.

The ^{19}F NMR spectrum at –46 °C of $N(CH_3)_4PF_4$ in CH$_3$CN containing a 3.7 M excess of $N(CH_3)_4F$ shows, in addition to a signal due to excess F$^-$, resonances attributable to PF$_4^-$, POF$_2^-$, and HPF$_5^-$. The latter two species comprised approximately 10–15% of the total phosphorus in the sample and are thought to have arisen from the adventitious hydrolysis of the PF$_4^-$ anion during synthesis or storage. The reactions giving rise to these products will be described in detail in a separate article.[36] The resonances arising from the PF$_4^-$ anion (Figure 3) comprise two doublets of triplets attributed to the axial (δ = 9.3 ppm) and equatorial (δ = –46.7 ppm) fluorine ligand environments, in accord with the pseudo trigonal bipyramidal structure for PF$_4^-$. The doublet splittings arise from the one-bond couplings $^1J(^{31}P–^{19}F_{ax})$ and $^1J(^{31}P–^{19}F_{eq})$ and are in agreement with those measured from the ^{31}P spectrum. The smaller triplet splittings arise from $^2J(^{19}F_{ax}–^{19}F_{eq})$ = 108 Hz. The chemical shift assignments are based on the magnitudes of the $^1J(^{31}P–^{19}F)$ values for each resonance. The magnitude of $^1J(^{31}P–^{19}F_{eq})$ is expected to be greater than that of $^1J(^{31}P–^{19}F_{ax})$ because of the higher s-character of the equatorial bonds. This agrees with the fact that the P–F$_{eq}$ bond length is shorter than the P–F$_{ax}$ bond length (see below). In the room temperature ^{19}F NMR spectrum of PF$_4^-$ the two doublets of triplets collapse into a single broad (half-width ∼ 400 Hz) line due to the above-mentioned axial–equatorial ligand exchange.

Vibrational Spectra. The infrared and Raman spectra of solid $N(CH_3)_4PF_4$ are shown in Figure 4, and the observed frequencies together with their assignments are summarized in Table 5. The bands due to PF$_4^-$ have been marked in Figure 4 with their frequency values. The remaining bands belong to the $N(CH_3)_4^+$ cation, and their assignments have previously been discussed and are well understood.[16,18] As can be seen from Figure 4, the Raman spectrum of $N(CH_3)_4PF_4$ is dominated by the cation bands, while in the infrared spectrum the PF$_4^-$ bands are more prominent.
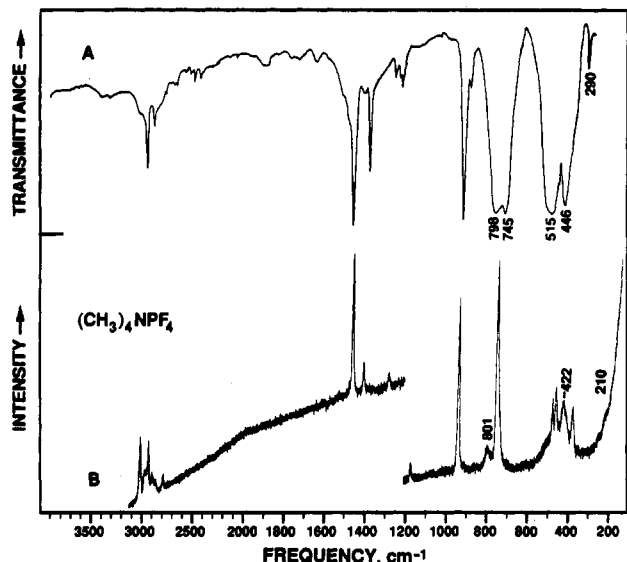
Tetrafluorophosphite, PF₄⁻, Anion

J. Am. Chem. Soc., Vol. 116, No. 7, 1994 2855

Figure 4. Infrared (trace A) and Raman (trace B) spectra of solid $N(CH_3)_4PF_4$.

Table 5. Vibrational Spectra of $N(CH_3)_4PF_4$ and Their Assignments

obsd freq, cm⁻¹ (rel int)		assignments (point group)	
IR	Ra	$N(CH_3)_4^+$ (T_d)	PF_4^- (C_{2v})
3500 vw			
3415 vw	▲		
3120 sh			
3043 m			
	3042 (30)	$\nu_5(E)$	
2975 w	2996 (10)	$\nu_{14}(F_2)$	
	2962 (23)	$\nu_1(A_1)$	
	2920 (7)	+ combin	
2780 vw	2895 sh	bands	
2755 vw	2813 (7)		
2663 vw			
2622 vw			
2585 w			
2521 vw			
1940 vw, br			
1815 vw			
1776 vw			
1686 vw			
1550 sh			
1493 s			
		$\nu_{15}(F_2)$	
1444 vw	1476 (73)	$\nu_2(A_1)$, $\nu_6(E)$	
1416 m	1419 (14)	$\nu_{16}(F_2)$	
1289 vw	1293 (6)	$\nu_{17}(F_2)$	
1263 vw			
1253 vw			
	1181 (8)	$\nu_7(E)$	
950 s	952 (82)	$\nu_{18}(F_2)$	
918 vw			
798 vs	801 (9)		$\nu_1(A_1)$
	758 (100) }	$\nu_3(A_1)$	
745 vs	745 sh }		$\nu_8(B_2)$
515 vs			$\nu_6(B_1)$
475 vw	476 (28) }	$\nu_{19}(F_2)$	
	459 (35) }		
446 s			$\nu_3(A_1)$, $\nu_7(B_1)$
	422 (25)		$\nu_2(A_1)$
	375 (22)	$\nu_8(E)$	
290 mw			$\nu_9(B_2)$
	210 (2)		$\nu_4(A_1)$

The bands due to the PF_4^- anion are summarized in Table 6. Their assignments in point group C_{2v} were made by comparison with those of isoelectronic SF_4[52] and with the frequencies

(52) Sawodny, W.; Birk, K.; Fogarasi, G.; Christe, K. O. *Z. Naturforsch., B* **1980**, *35B*, 1137 and references cited therein.

calculated for PF_4^- (see below). Their agreement is satisfactory. As expected, the formal negative charge in the PF_4^- anion increases the negative charge on the fluorine ligands and, hence, the $(\delta+)P–F(\delta-)$ bond polarity. This results in a general lowering of the frequencies and stretching force constants relative to the neutral SF_4 molecule.

A comparison of our infrared spectrum for PF_4^- in $N(CH_3)_4$-PF_4 with that attributed by Wermer and Ault to a $Cs^+PF_4^-$ ion pair in an argon matrix[15] shows only little similarity. This implies that PF_4^- in the two species is either very different or that the species observed in the matrix might not have been PF_4^-.

Theoretical Calculations and Normal Coordinate Analyses. The electronic structure of PF_4^- was calculated using both local (LDF) and nonlocal (NLDF) density functional theories and molecular orbital theory at the self-consistent field (SCF) and MP2 levels. All calculations resulted in a pseudo trigonal bipyramidal structure of C_{2v} symmetry as the minimum energy structure (see Table 7). To obtain a better feel for the quality of these calculations, the well-known PF_3 molecule[53-55] was also calculated by the same methods. As can be seen from Table 8, the SCF calculation duplicates best the experimental geometry and vibrational frequencies of PF_3. Therefore, the SCF values are also preferred for PF_4^- and are in good agreement with the experimentally observed values (see Table 7). This good agreement clearly demonstrates that the geometries of PF_4^- in solid $N(CH_3)_4PF_4$ and that calculated for the free ion must be very similar, indeed.

The geometry parameters, calculated for PF_4^- at different levels of theory (see Table 7), show some interesting trends. Correlation effects are significant and at the MP2 level lengthen $r(P–F_{eq})$ by 0.05 Å and the already longer $P–F_{ax}$ bond by a somewhat smaller value of 0.03 Å. The LDF calculations show bond lengths comparable to those obtained at the MP2 level. Inclusion of self-consistent nonlocal effects increases both the axial and equatorial bond lengths with the larger effect on the axial bond. Comparison of our calculations with those[56] previously carried out by O'Keeffe using a 631G* basis set shows that the results agree within 0.01 Å. The HFS/LDF results[57] of Gutsev are also in reasonable agreement with our LDF results, considering the differences in the basis sets, method, and local potential.

A normal coordinate analysis was carried out for PF_4^-. The internal and symmetry coordinates and the explicit F matrix used were identical to those previously published[52] for isoelectronic SF_4. The nine fundamental vibrations of PF_4^- of C_{2v} symmetry can be classified as $\Gamma = 4A_1(IR,Ra) + A_2(Ra) + 2B_1(IR,Ra) + 2B_2(IR,Ra)$, whereby the B_2 modes were arbitrarily chosen to be symmetric to the symmetry plane defined by the equatorial PF_2 group. Since the scaled SCF frequencies of PF_4^- duplicate best the experimentally observed ones, the scaled SCF force field was used and is given in Table 9. The potential energy distribution (PED) is shown in Table 10. The internal stretching force constants of PF_4^- are given in Table 11 and are compared to those of isoelectronic SF_4[52] and the phosphorus fluorides PF_3,[55,58,59] PF_6^-,[60] and PF_5.[61,62]

The results of the normal coordinate analysis demonstrate that, by analogy with isoelectronic SF_4,[52] the symmetric equatorial and axial bending motions, $\nu_3(A_1)$ and $\nu_4(A_1)$, are highly mixed,

(53) Morino, Y.; Kuchitsu, K.; Moritani, T. *Inorg. Chem.* **1969**, *8*, 867.

(54) Hirota, E.; Morino, Y. *J. Mol. Spectrosc.* **1970**, *33*, 460. Kawashima, Y.; Cox, A. P. *J. Mol. Spectrosc.* **1977**, *65*, 319.

(55) Reichman, S.; Overend, J. *Spectrochim. Acta, Part A* **1970**, *26A*, 379. Reichman, S. *J. Mol. Spectrosc.* **1970**, *35*, 329. Small, C. E.; Smith, J. G. *J. Mol. Spectrosc.* **1978**, *73*, 215.

(56) O'Keeffe, M. *J. Am. Chem. Soc.* **1986**, *108*, 4341.

(57) Gutsev, G. L. *J. Chem. Phys.* **1993**, *98*, 444.

(58) Breidung, J.; Thiel, W. *J. Comput. Chem.* **1992**, *13*, 165.

(59) Breidung, J.; Schneider, W.; Thiel, W. *J. Mol. Spectrosc.* **1990**, *140*, 226.

(60) Sawodny, W. Habilitation Thesis, University of Stuttgart, Germany, 1969.

(61) Marsden, C. J. *J. Chem. Phys.* **1987**, *87*, 6626.

(62) Christen, D.; Kadel, J.; Liedtke, A.; Minkwitz, R.; Oberhammer, H. *J. Phys. Chem.* **1989**, *93*, 6672.

Table 6. Comparison of Observed and Calculated Frequencies of PF_4^- with Those of SF_4 and Their Approximate Mode Descriptions

assignment in point group C_{2v}		approximate mode description	PF_4^- obsd freq, cm⁻¹(int) IR	Ra	calcd freq,[a] (IR int) SCF	SF_4 obsd freq, cm⁻¹(int) IR	Ra
A_1	ν_1	ν sym $XF_{2,eq}$	798 vs	801 ms	795 (218)	892 s	893 (92)
	ν_2	ν sym $XF_{2,ax}$		422 s	416 (0)	558 w	558 (100)
	ν_3	δ sciss $XF_{2,eq,ax}$, sym comb	446 s		464 (28)	532 ms	535 (35)
	ν_4	δ sciss $XF_{2,eq,ax}$, asym comb		210 sh	201 (1.0)	226 w	229 (10)
A_2	ν_5	XF_2 twist			392 (0)		
B_1	ν_6	ν asym $XF_{2,ax}$	515 vs		523 (620)	728 vs	730 (5)
	ν_7	δ wag $XF_{2,eq}$	446 s		446 (56)		474 (7)
B_2	ν_8	ν asym $XF_{2,eq}$	745 vs		746 (209)	867 s	865 sh
	ν_9	δ sciss $XF_{2,ax}$ out of plane	290 mw		293 (7.4)	353 m	356 (0+)

[a] The frequency values were scaled by an empirical factor of 0.9005 to maximize the fit with the observed values.

Table 7. Geometries and Vibrational Frequencies Calculated for PF_4^- by Different Methods

computational method	geometry $r_{PF_{eq}}$ (Å)	$r_{PF_{ax}}$ (Å)	F_{eq}-P-F_{eq} (deg)	$\angle F_{ax}$-P-F_{ax} (deg)	$\angle F_{eq}$-P-F_{ax} (deg)	vibrational freq (cm⁻¹) and relative infrared intensity $\nu_1(A_1)$	$\nu_2(A_1)$	$\nu_3(A_1)$	$\nu_4(A_1)$	$\nu_5(A_2)$	$\nu_6(B_1)$	$\nu_7(B_1)$	$\nu_8(B_2)$	$\nu_9(B_2)$
SCF[a]	1.604	1.741	99.9	168.3	86.2	795 (218)	416 (0)	464 (28)	201 (1.0)	392 (0)	523 (620)	446 (56)	746 (209)	293 (7.4)
MP2[b]	1.651	1.774	98.9	169.7	86.7	808 (174)	461 (2.4)	453 (15)	200 (0.9)	384 (0)	602 (588)	442 (7.2)	750 (188)	285 (6.0)
LDF[b]	1.666	1.768	98.2	169.8	86.7	757	451	408	178	349	607	405	709	261
NLDF/BP[b]	1.673	1.814	99.2	171.0	87.1	735 (168)	405 (3.9)	394 (7.3)	177 (1.3)	344 (0)	537 (547)	390 (27)	673 (252)	252 (5.1)
exptl values		1.73(1)				801 vs	422 (Ra)	446 s	210 (Ra)		515 vs	446 s	745 vs	290 mw

[a] The frequency values were scaled by an empirical factor of 0.9005 to maximize the fit with the observed values. [b] Unscaled frequencies.

Table 8. Experimental and Calculated Geometries and Vibrational Frequencies of PF_3

computational method	geometry r_{PF} (Å)	$\angle FPF$ (deg)	vibrational freq (cm⁻¹) and relative infrared intensity $\nu_1(A_1)$	$\nu_2(A_1)$	$\nu_3(E)$	$\nu_4(E)$
SCF[a]	1.562	97.2	896 (182)	486 (43)	859 (468)	347 (15)
MP2[b]	1.602	97.4	884 (143)	465 (30)	853 (418)	330 (12)
LDF[b]	1.616	96.9	834	420	823	300
NLDF/BP[b]	1.622	97.6	813 (134)	431 (21)	780 (420)	206 (8)
exptl values	1.561(1)	97.7(2)	892 s	488 m	860 vs	347 w

[a] Frequency values scaled by an empirical factor of 0.9283 to maximize the fit between calculated and experimental values. [b] Unscaled frequencies.

Table 9. Symmetry Force Constants[a] of PF_4^- Calculated from the Scaled SCF Frequencies of Table 8
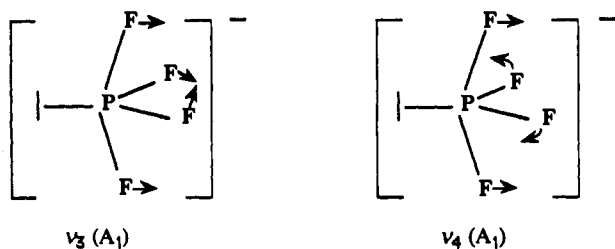
	F_{11}	F_{22}	F_{33}	F_{44}		F_{66}	F_{77}
F_{11}	4.204				F_{66}	1.484	
F_{22}	0.721	2.159			F_{77}	0.577	1.679
F_{33}	0.303	−0.055	1.152			F_{88}	F_{99}
F_{44}	0.163	0.034	0.489	1.078	F_{88}	3.676	
F_{55}	1.482				F_{99}	−0.328	1.524

[a] Stretching constants in mdyn/Å, deformation constants in mdyn Å/rad², and stretch–bend interaction constants in mdyn/rad.

Table 10. Potential Energy Distribution for PF_4^-

		freq, cm⁻¹	PED, %
A_1	ν_1	795	60.2(1) + 20.5(3) + 15.7(4) + 3.6(2)
	ν_2	416	91.7(2) + 7.8(2) + 0.5(4)
	ν_3	464	50.2(3) + 45.5(4) + 4.0(1) + 0.3(2)
	ν_4	201	52.7(4) + 46.9(3) + 0.3(2) + 0.1(1)
A_2	ν_5	392	100(5)
B_1	ν_6	523	57.8(6) + 42.2(7)
	ν_7	446	57.2(7) + 42.8(6)
B_2	ν_8	746	89.9(8) + 10.1(9)
	ν_9	293	99.7(9) + 0.3(8)

Table 11. Stretching Force Constants (mdyn/Å) of PF_4^- Compared to Those of SF_4, PF_3, PF_6^-, and PF_5

	SF_4[a]	PF_4^-	PF_3[b]	PF_6^-[c]	PF_5[d]
$f_{r,eq}$	5.405	3.940	5.470	4.02	6.47
f_{rr}	0.240	0.264	0.449		
$f_{R,ax}$	3.150	1.822			5.45
f_{RR}	0.329	0.338			

[a] Values from ref 52. [b] Values from refs 55, 58. [c] Values from ref 60. [d] Values from ref 62.

with ν_3 being a symmetric combination and ν_4 being an antisymmetric combination of the corresponding symmetry coordinates.

ν_3 (A_1) ν_4 (A_1)

The $\nu_4(A_1)$ mode has the lowest frequency of all the PF_4^- modes and represents the motion involved in the Berry pseudorotation mechanism (see above). Its frequency is comparable with but slightly lower than that in SF_4 and supports the conclusion from our NMR study (see above) that the activation energies for the intramolecular exchange in these two species have similar values. The fact that ν_6 and ν_7 in the B_1 block are also almost equal mixtures of the corresponding symmetry coordinates differs from SF_4 and is due to the more similar frequency values of ν_6 and ν_7 in PF_4^-.

To verify the Berry pseudorotation mechanism, we have also calculated the C_{4v} structure of PF_4^- at the SCF level and obtained an MP2 energy for this geometry. The C_{4v} structure is a transition state with an imaginary frequency of 174i cm⁻¹. The P–F bond distance is 1.675 Å, and the F–P–F bond angle is 82.1°. The C_{4v}

Tetrafluorophosphite, PF₄⁻, Anion

J. Am. Chem. Soc., Vol. 116, No. 7, 1994 2857
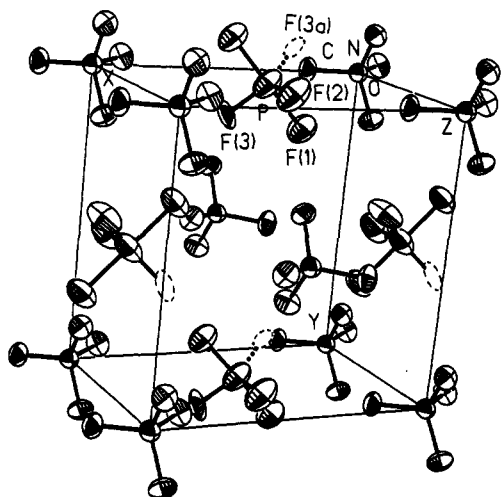
Figure 5. ORTEP drawing of the unit cell of $N(CH_3)_4PF_4$ showing the packing of the PF_4^- anions and $N(CH_3)_4^+$ cations with thermal ellipsoids drawn at the 50% probability.

structure is 48.7 kJ mol⁻¹ above the C_{2v} structure at the SCF level and 43.7 kJ mol⁻¹ higher at the MP2 level. These values are in excellent agreement with the experimental value of 43.5 kJ mol⁻¹ for $\Delta H^\ddagger$.

The large differences between the equatorial and the axial stretching force constants, f_r and f_R, respectively, in PF_4^- and SF_4 are in agreement with the observed large differences in bond lengths and can be rationalized in terms of semi-ionic, three-center four-electron bonding for the axial fluorine ligands. The high polarity of the bonds in PF_4^- also explains why the equatorial stretching force constant in PF_4^- (3.94 mdyn/Å) is significantly smaller than that found for PF_3 (5.47 mdyn/Å).[55,58] The same effect of bond weakening by the formal negative charge is found for the PF_5–PF_6^- couple (see Table 11). The higher force constants in the (+V) phosphorus compounds, when compared to those in the corresponding (+III) compounds, is due to the increased effective electronegativity of the central atom and the resulting decrease in polarity of the P–F bonds. The stretch–stretch interaction constants, f_{rr} and f_{RR}, in PF_4^- and SF_4 also have very similar values (see Table 11) and provide further evidence for the pronounced similarity of these two isoelectronic species.

X-ray Crystal Structure of $N(CH_3)_4PF_4$. The crystal structure consists of well-separated $N(CH_3)_4^+$ and PF_4^- ions and can be derived from a primitive cubic CsCl-type structure in which the cube formed by the cations is regular, while the cube formed by the anions is somewhat distorted (see Figure 5). The volume of the unit cell is 27 Å³ smaller than that determined for $N(CH_3)_4$-PF_6 at the same temperature.[63] It is generally accepted that the effective volume of a lone pair is only slightly smaller than that of a fluorine atom (i.e., 20 Å³).[64] Consequently, the expected volume difference between $N(CH_3)_4PF_6$ and $N(CH_3)_4PF_4$ should be slightly larger than 20 Å³, as was observed.

The $N(CH_3)_4^+$ cation is tetrahedral with the expected C–N bond lengths (1.505(6) Å) and C–N–C angles (109.5(2)°). The gross geometry of the PF_4^- anion can be described as a pseudo trigonal bipyramid in which (i) the lone valence electron pair of phosphorus and two fluorines occupy the equatorial positions and (ii) the axial P–F bonds are longer than the equatorial P–F bonds (Figure 5).

The disorder of the PF_4^- anion in its equatorial plane involves two fluorine ligands and one sterically active free valence electron pair, which can be considered much shorter and more repulsive than a P–F bond. Therefore, the apparent equatorial bond lengths,

resulting from the averaging of P–F bonds with the free pair, are too short for normal P–F bonds, and the apparent bond angles also deviate significantly from the theoretical predictions for ordered PF_4^- (see Theoretical Calculations section). As can be seen from Table 3, the observed apparent geometry of ordered PF_4^- is intermediate between those derived from subjecting the free ordered ion to either 2-fold or 3-fold disorder with equal occupancy factors. Therefore, the crystal structure of $N(CH_3)_4$-PF_4 is best interpreted in terms of a mixture of 2-fold and 3-fold disorder, which amounts to a 3-fold disorder with unequal occupancy factors. A minimum R-value was obtained for the set of occupancy factors listed in Table 2. The superposition of the different equatorial positions results in close, but distinct, positions for the F(3) atom, as reflected in the large value for the thermal parameters, U_{33} = 0.159 Å² (supplementary Table 2) and the correspondingly large correction for libration for the P–F(3) bond length (Table 3). The positional disorder of the F(3) atoms is
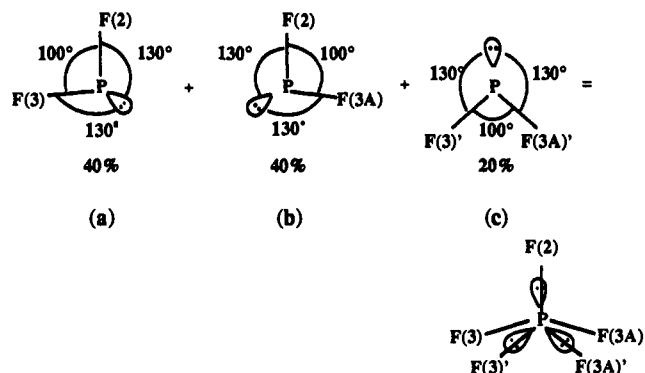
also responsible for the apparent equatorial F–P–F bond angle to be larger than 100°.

In view of the disorder of PF_4^- in $N(CH_3)_4PF_4$, only the axial P–F bond length is well determined by the X-ray data. The remaining geometrical parameters of PF_4^- are strongly influenced by the disorder, but are consistent with the theoretically calculated structure assuming 3-fold disorder with unequal occupancy factors. In view of this consistency and the agreement between the calculated and observed axial bond length and vibrational frequencies (see above), the structure of PF_4^- is best described by the following geometry.
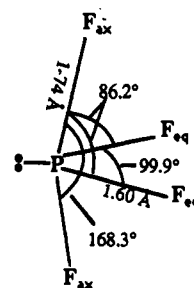
It is interesting to compare this geometry with those established for other similar molecules and ions. As can be seen from Table 12, the geometry of PF_4^- is very similar to that[65] of isoelectronic SF_4, with the bonds in PF_4^- being slightly longer, as has been discussed before. The increased length of the axial bonds over that of the equatorial bonds is consistent with the hypervalent nature of these pseudo trigonal bipyramidal compounds and with strong contributions from semi-ionic, three-center four-electron bonding[66] to the axial bonds. Furthermore, the fact that the axial fluorine ligands are bent away from the sterically active

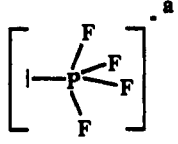(63) Wang, Y.; Calvert, L. D.; Brownstein, S. K. *Acta Crystallogr.* **1980**, *B36*, 1523.
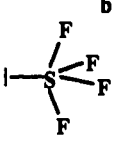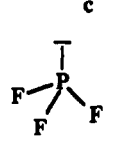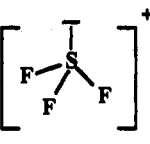
(64) (a) Zachariasen, W. H. *J. Am. Chem. Soc.* **1948**, *70*, 2147. (b) Edwards, A. J.; Sillos, R. J. C. *J. Chem. Soc. A* **1971**, 942.

(65) Tolles, W. M.; Gwinn, W. D. *J. Chem. Phys.* **1962**, *36*, 1119.

(66) Pimentel, G. C. *J. Chem. Phys.* **1951**, *19*, 446. Hach, R. J.; Rundle, R. E. *J. Am. Chem. Soc.* **1951**, *73*, 4321. Rundle, R. E. *J. Am. Chem. Soc.* **1963**, *85*, 112.

Table 12. A Comparison of the Geometry of PF_4^- with Those of Closely Related Molecules and Ions

	a	b	c	d
$X\text{-}F_{ax}$	1.74	1.646(3)		
$X\text{-}F_{eq}$	1.60	1.545(3)	1.570(1)	1.515(2)
$F_{ax}\text{-}X\text{-}F_{ax}$	168.3	173.1(5)		
$F_{eq}\text{-}X\text{-}F_{eq}$	99.9	101.6(5)	97.8(2)	96.2(1)

a Values from our SCF calculation. *b* Data from ref 65. *c* Data from ref 53. *d* Data from ref 63.

free valence electron pair in the equatorial plane is in accord with the increased repulsion from a free valence electron pair and the VSEPR rules.[37,38] The equatorial bonds in PF_4^- are also somewhat longer than those[53] in PF_3, which again can be attributed to the formal negative charge on PF_4^-. Finally, the isoelectronic pairs, PF_4^-–SF_4 and PF_3–SF_3^+,[67] exhibit about the same amount of bond shortening (~0.06 Å) on going from the phosphorus to the sulfur species.

The cation–anion interactions in $N(CH_3)_4PF_4$ were also examined and show four short P- - -C contacts (supplementary Figure S1) of 3.95 Å (sum of the CH_3 and P van der Waals contacts, 3.85 Å[68,69]) and sixteen short F- - -C contacts (four per fluorine atom) ranging from 3.29 to 3.53 Å (sum of the CH_3 and F van der Waals contacts, 3.35–3.40 Å[68,69]). The nearest neighbor P- - -F contacts of 4.42 Å (sum of the P and F van der Waals contacts, 3.20–3.25 Å[69]) preclude Hal- - -P- - -Hal bridge interactions, which have been observed for $N(n\text{-}C_3H_7)_4^+PBr_4^-$[5] but not for $N(C_2H_5)_4^+PCl_4^-$.[7]

The successful synthesis and characterization of the PF_4^- anion completes the PF_4^-,PCl_4^-,PBr_4^- triad. The structures of the PCl_4^- and PBr_4^- anions are unusual because their axial Hal–P–Hal groups are easily distorted. For example, in $N(nPr)_4PBr_4$, the PBr_4^- anion has an almost ideal pseudo trigonal bipyramidal C_{2v} structure,[5] while in $N(C_2H_5)_4PBr_4$, its structure is better described as one of a PBr_3 molecule with a loosely attached fourth Br^- ion.[6]

Obviously, the energy difference between the symmetric and the asymmetric PBr_4^- structures must be very small, and their geometries are influenced by effects such as the size of the counter cation and crystal packing. In $N(C_2H_5)_4PCl_4$, the asymmetry of the axial PCl_2 group is even more pronounced (2.118(4) and 2.850(4) Å[7]) and, by extrapolation, one might predict that, on going from PBr_4^- and PCl_4^- to PF_4^- and from $N(C_2H_5)_4^+$ to the even smaller $N(CH_3)_4^+$ counter cation, the asymmetry of the

axial phosphorus–halogen bonds should further increase. This, however, is not the case; the axial P–F bonds in $N(CH_3)_4PF_4$ are perfectly symmetric, and the PF_4^- anion closely resembles the isoelectronic SF_4 molecule, with both undergoing facile equatorial–axial ligand exchanges with comparable activation enthalpies. It appears that the chemical and physical properties of PF_4^- and PCl_4^- closely follow those of isoelectronic SF_4 and SCl_4. Sulfur tetrafluoride is a covalent, stable molecule, while SCl_4 decomposes at –31 °C and, as a solid, probably has the ionic structure $SCl_3^+Cl^-$.[70–72] The fact that in the chlorides the energy difference between the covalent, pseudo trigonal bipyramidal C_{2v} structure and the more ionic X- - -MX_3 C_{3v} structure is quite small while in the fluorides it is large has recently been also demonstrated by Gutsev through local density functional method calculations for PF_4^- and SCl_4.[57,73]

Supplementary Material Available: A structure determination summary (Table S1), tables of anisotropic thermal paramters and hydrogen atomic coordinates (Tables S2 and S3), a drawing showing the shortest P- - -C contacts (Figure S1) (5 pages); tabulation of calculated and observed structure factor amplitudes (Table S4) (1 page). This material is contained in many libraries on microfiche, immediately follows this article in the microfilm version of the journal, and can be ordered from the ACS; see any current masthead page for ordering information.

(67) Mallouk, T. E.; Rosenthal, G. L.; Müller, G.; Brusasco, R.; Bartlett, N. *Inorg. Chem.* **1984**, *23*, 3167.

(68) Pauling, L. *The Nature of the Chemical Bond*, 3rd ed.; Cornell University Press: Ithaca, NY, 1960; p 261.

(69) Bondi, A. *J. Phys. Chem.* **1964**, *68*, 441.

(70) Steudel, R.; Jensen, D.; Plinke, B. *Z. Naturforsch., B* **1987**, *42*, 163.

(71) Kniep, R.; Korte, L.; Mootz, D. *Z. Naturforsch., B* **1984**, *39*, 305.

(72) Greenwood, N. N.; Earnshaw, A. *Chemistry of the Elements*; Pergamon Press: Oxford, 1989; p 816.

(73) Gutsev, G. L. *J. Phys. Chem.* **1992**, *96*, 10242.